Pulmonary Matrix Derived Hydrogels from Patients with Idiopathic Pulmonary Fibrosis Induce a Proinflammatory State in Lung Fibroblasts In Vitro

Authors: Fernandez Davila JG[1], Moore DW[1], Kim J[1], Khan JA[1], Singh AK[2,3], Lemma M[4], King CS[4], Nathan SD[4], Rodriguez LR[1*], Grant GM[1 *], Moran JL[2,3 *].

1: Department of Biology, George Mason University, 10900 University Blvd., Manassas VA 20110 USA
2: Department of Mechanical Engineering, George Mason University, 10920 George Mason Circle, Manassas VA 20110 USA
3: Department of Bioengineering, George Mason University, 10920 George Mason Circle, Manassas VA 20110 USA
4: Inova Advanced Lung Disease and Transplant Program, Inova Fairfax Hospital, 3300 Gallows Road, Falls Church VA 22042 USA

*: Senior Authors Contributed Equally

Corresponding Authors:	Jeffrey L Moran, PhD
Address:	Department of Mechanical Engineering George Mason University, 10920 George Mason Cir, Manassas VA 20110 USA
Telephone:	1-703-993-5636
Email address:	jmoran23@gmu.edu
	Geraldine Grant, PhD
Address:	Department of Biology George Mason University, 10900 University Blvd., Manassas VA 20110 USA
Telephone:	1-703-993-5636
Email address:	ggrant1@gmu.edu

ABSTRACT

Idiopathic pulmonary fibrosis (IPF), one of the most common forms of interstitial lung disease, is a poorly understood and fatal condition with only two FDA-approved medications. As a chronic fibroproliferative disorder, the pathobiology of the fibroblast in IPF is critical to the evaluation and discovery of novel therapeutics. Unfortunately, our ability to interrogate this biology *in vitro* is greatly limited by the well-documented effect of tissue culture plastic on the fibroblast phenotype. Using decellularized IPF-derived lung matrix, we characterize the phenotype of fibroblasts seeded into three-dimensional (3D) fibrotic hydrogels. We identify differential gene expression and differential contractility in IPF fibroblasts as compared to their normal counterparts. Additionally, fibroblasts seeded into these matrices lose the classical myofibroblast marker, smooth muscle actin, and gain significant expression of proinflammatory cytokines compared to 2D tissue culture dishes. In a series of co-culture studies with monocytes and monocyte- derived macrophages, we validate this proinflammatory state. The application of this 3D fibrotic hydrogel model for the potential intervention in disease associated fibroblast-immune cell crosstalk may uncover a novel therapeutic avenue. These findings add to a growing understanding of the lung microenvironment effect on fibroblast phenotypes and shed new light on the potential role of fibroblasts as immune signaling hubs during lung fibrosis.

Keywords: Pulmonary Fibrosis, Decellularized Matrix, Mechanobiology, Three-dimensional, Culture, Fibroblast-Immune Crosstalk

INTRODUCTION

Idiopathic pulmonary fibrosis (IPF) is a chronic fibroproliferative disease characterized by dysregulated wound healing and severe scarring in the lung[1,2]. The molecular mechanism underlying wound healing is a tightly regulated sequential cycle of inflammation, proliferation and remodeling that, when disrupted, results in the progressive development of scarring, tissue stiffening, and physiological restriction[3,4]. The remodeling of the pulmonary extracellular matrix (ECM) orchestrated by lung resident fibroblasts is critical to the progression of fibrotic diseases such as IPF. These fibroblasts and their activity have been the primary target of the only two small-molecule therapeutics, the antifibrotics Nintedanib and Pirfenidone, with FDA approval to treat IPF[5–7]. Despite the approved use of these compounds in 2014, their efficacy is limited and their side effects are often severe [6,8–11]. Moreover, there are only a small handful of compounds in Phase III clinical trials, suggesting gaps in IPF drug delivery and design[8]. Specifically, the lack of physiological mimicry by *in vitro* model systems has greatly reduced our ability to test and produce efficacious FDA-approved therapies[12].

Many discovery programs for antifibrotic therapy begin with 2-dimensional (2D) tissue cultures *in vitro*; however, a major disadvantage of 2D cultures is the absence of cell-ECM interactions which are pivotal for cell differentiation, gene and protein expression, responsiveness to stimuli, and other important cellular functions during fibrosis[13–15]. We have previously demonstrated that both fibroblasts extracted from patients with advanced stage IPF (IPF-F) and normal human lung fibroblasts (NHLF) undergo a dramatic phenotypic change when removed from the complex lung microenvironment and transferred to stiff tissue culture plastic[16,17]. During the preclinical phase of therapeutic development, it is critical to assess diseased cells in an environment that replicates pathological hallmarks, including mechanical signals from the stiff ECM[3,18,19]. Recent advancements in *in vitro* disease models have improved our understanding as to how fibroblasts interact with ECM components, enzymes, and different cell types *in*

vivo[20,21]*.* The behavior of fibroblasts is also dictated by the complex interplay of biological features such as integrin binding sites, ECM mechanical properties, and chemical cues elicited by immune cells[13,14,22]. Beyond the fibroblast, immune cells such as macrophages have been recognized to play a significant role in IPF pathogenesis. Macrophages are one of the main reservoirs of profibrotic cytokines including transforming growth factor beta (TGFβ), a primary effector molecule in fibrosis regulating fibroblast activation[23–25]. Macrophages, derived from circulating monocytes and accumulating in the IPF microenvironment, have been implicated in the pathogenesis of IPF[23,24,26–28]. These interactions can be studied *in vitro* with co-culture platforms such as 3D collagen co-cultures[29]. These matrices form a highly relevant biomimetic model of paracrine communication in wound healing[29]. Replicating the mechanical and three-dimensional properties of native lung ECM along with robust fibroblast and immune cell co-culture systems are essential to accurately model the fibrotic microenvironment *in vitro* for therapeutic discovery.

In the past few decades, *in vitro* models have been improved to meet the challenge of modeling complex *in vivo* systems. For example, 3D collagen hydrogel models with tunable mechanical stiffness have been applied to elucidate fibroblasts' mechanoregulation[3,13,15,19]. Collagen, however, is only one example of a material used to generate a 3D system. Currently, models range from naturally derived native ECM components to synthetic tunable materials that more closely resemble the *in vivo* mechanical environment[3,13,30]. These models have demonstrated that fibroblasts modeled in 3D transition into a quiescent state that phenocopies fibroblasts' activity *in vivo*, prior to activation and entry into wound healing[13,31]. Overall, the development of *in vitro* 3D hydrogels for fibroblast research is an effective and necessary method of enriching the environment in which fibroblasts are cultured[14].

The extended characterization of fibroblast biology in collagen and polymer-based 3D hydrogels has recently allowed for the description of understudied disease relevant properties such as fibroblast contractility [32–34]. These 3D models demonstrate that hydrogel contraction increases in the presence of pro-fibrotic mediators such as TGFβ, and that this contraction can be reduced using Nintedanib and Pirfenidone[33]. Beyond these antifibrotics, the application of anti-inflammatory compounds, specifically interleukin 4 (IL-4) and interleukin 6 (IL-6) inhibitors, can also reduce hydrogel contraction[32,34]. It is evident that hydrogels are a suitable platform to investigate fibroblasts and fibrosis; however, this approach is in its infancy and has yet to be fully optimized.

To further overcome the limitations of *in vitro* drug discovery and disease characterization, we present a 3D model of IPF patient-derived hydrogels which, compared to 2D tissue culture plastic, more closely resembles the fibrotic lung environment. During our characterization of our IPF ECM derived hydrogels, we observed that fibroblasts in 3D have exhibited significant decrease of fibroblast activation and proliferation compared to fibroblasts on 2D tissue culture dishes. Additionally, these fibroblasts demonstrate differential cytokine signaling compared to 2D culture, which suggests a potential application for the interrogation of fibroblast-macrophage crosstalk. By characterizing how fibroblasts behave in our patient-derived model of fibrotic lung, we aim to expand knowledge and provide novel *in vitro* tools for the development of therapies to treat IPF.

METHODS

Donor consent and internal review board approval

This study was conducted in accordance with principles set forth by the Declaration of Helsinki. IPF lung tissue was obtained through Inova Fairfax Hospital (VA). All normal control lungs were obtained through the Washington Regional Transplant Community (WRTC). Appropriate written

informed consent was obtained from each patient and donor by Inova Fairfax Hospital and the WRTC. This study was approved by the Inova Fairfax Hospital Internal Review Board (IRB #06.083) and the George Mason University Human Subject Review Board (Exemption #5022). All experiments were performed in accordance with relevant guidelines and regulations.

Tissue Decellularization

This protocol is adapted from a previously published protocol [35] and summarized in Figure 1. IPF lung tissue (n=4) was minced into 2-5 mm^3 pieces and then washed with the following solutions at room temperature for 24 h each replacing the solution three times: 1% sodium dodecyl sulfate (SDS) solution in water followed by 1% Triton X-100 solution in water. The tissue was then rinsed twice with 1X phosphate buffered saline (PBS) and washed with the following solutions for 30 min each with two rinses of PBS and seven rinses of water in between: 10 U/mL of DNase in 1X PBS at 37°C, 1 M NaCl for 1 h, and 70% ethanol finalized with all rinses. Scaffold was maintained in PBS solution at 4°C until lyophilization.

Synthesis of ECM hydrogel

IPF lung scaffold was frozen for 10-16 h at -80°C prior to lyophilization. Frozen scaffold was then lyophilized overnight in a Millrock Technology Benchtop Manifold Freeze Dryer. Post-lyophilization, the sample was pulverized with a Spex SamplePrep Freezer/Mill 6875. Powdered lung scaffold was then digested by mixing 200 mg of scaffold powder and 100 mg of pepsin (MP Bio, 02102598-CF) (2:1 ratio) in 20 mL of hydrochloric acid (HCl) at pH 2.0 for 72 h. The pH of the solution was measured at the beginning of the digestion and once every 24 h for a period of 72 h; it was adjusted to pH 2.0 by droplet addition of 12 M HCl. The ECM solution was then neutralized to pH 7.0 with 1 M NaOH and dialyzed with water changed every hour for 3 times and left dialyzing overnight. The solution was transferred to a conical tube and frozen at -80°C overnight followed by a lyophilization for 24 h. The final product has the consistency of a

spongelike material that was resuspended in cell culture medium of choice at the desired concentration to form a pre-gel solution. Pre-gel solution is a viscous fluid which is pipetted into a well dish and incubated at 37°C for at least 45 min before reaching gelation. A graphical depiction of the process in presented in Figure 1.

Specimen procurement/dissection and cell culture

The primary fibroblasts used in this study were isolated from human lungs procured in the operating room within minutes of explantation. The lungs were oriented from apex to base, and all samples used in this study were taken from the peripheral lower lobe of the lung. Fibroblasts were isolated from the lung tissue of patients with advanced stage IPF (IPF-F) and normal healthy lungs (NHLF) using differential binding as previously described . IPF-F (n=5) and NHLF (n=4) were used in this study. Fibroblasts were cultured in a T-75 flask in Dulbecco's Modified Eagle Medium (DMEM) (Cytiva, SH30081.05) with 5% fetal bovine serum (FBS) and 1% penicillin/streptomycin, penicillin (100 I.U/mL) and streptomycin (100 MCH/mL) (Corning, 30-002-CI). Cells were cultured at 37°C using 5% CO_2. Passages of fibroblasts used for this analysis ranged from 4-7. U937 cells (ATCC, CRL-1593.2) were cultured in a T-75 flask using RPMI (ThermoFisher, 11875093) 1640 medium with 10% FBS and 1% penicillin/streptomycin and maintained in a humid incubator at 37°C using 5% CO_2. U937 cells were differentiated to macrophages through a 48-h incubation with 100 ng/mL of phorbol myristate acetate (PMA) (MP Bio, 02151864-CF).

IPF hydrogel cultures and conditioned media experiments

Fibroblasts were split/passaged when cells reached ~80% confluency using 0.05% trypsin/EDTA (ThermoFisher, 25300054) and pelleted at desired cell density. For regular tissue culture, fibroblasts were seeded in a 6-well dish with 2 mL of DMEM complete medium and cultured in the incubator for two days. For IPF hydrogel culture, fibroblasts were pelleted at 4 ×

10^5 cells per gel and slowly resuspended in the 600 µL pre-gel solution. The pre-gel with the cell suspension was then pipetted at a volume of 300 µL into a 48-well tissue culture dish and placed in a humidified incubator at 37°C with 5% CO_2 for 30 minutes to allow gelation before adding 500 µL of DMEM complete medium warmed to 37°C and placing the culture dish in the incubator.

For the co-culture experiments, conditioned media from fibroblasts was collected and spun at 1000 rpm for 5 min to leave behind any cell debris and/or floating cells. Conditioned media was used to challenge 5×10^5 U937 cells per gel on a 24-well tissue culture dish for 48 h. For PMA treatments, 2.5×10^5 U937 cells were seeded with 100 ng/mL PMA supplemented RMPI media and cultured for 48 h followed by RNA isolation. PMA media was removed and attached cells were washed with PBS followed by treatment with fibroblast conditioned media for 48 h and followed by RNA isolation.

RNA isolation and cDNA synthesis

RNA was isolated from IPF-F, NHLF, and U937 cells using the Omega Biotek E.Z.N.A Total RNA Kit I (Omega Biotek, R6834-02). For 3D cell extractions, hydrogel was incubated in complete media with 1% collagenase type I (ThermoFisher, 17100017) for 25-30 minutes. Once the cells disassociated from the hydrogel, solution was vigorously pipetted until hydrogel clumps were no longer visible. The solution was then centrifuged for 5 min at 1000 rpm, and the pellet was resuspended in lysis buffer followed by isolation according to manufactures instructions. For analysis, 0.1-0.2 µg of RNA was converted to cDNA using the VERSO cDNA Synthesis Kit (ThermoFisher, AB1453A) prior to quantitative PCR.

Realtime Quantitative PCR

Quantitative PCR (qPCR) was performed in a Bio-Rad CFX Connect Optics Module by using the Applied Biosystems Fast SYBR Green Master Mix kit (ThermoFisher, 4385612). qPCR was normalized to 18S expression using the delta-delta Ct method[36]. Statistical analysis for Figure 3 was performed via paired T-test in Microsoft Excel. Welch's T-test was performed via GraphPad Prism 9 for Figure 4. One-way ANOVA was performed via GraphPad Prism 9 for Figures 5 and 6. Expression fold differences with p-values less than 0.05 were considered significant.

Microscopy and Hydrogel Contraction Analysis

Images of hydrogels were captured with a Life Technologies EVOS FL Auto imaging system in the 48-well vessel layout taken at 4X magnification. Contractility of hydrogels was analyzed by measuring the reduction in surface area of the contracted hydrogel touching the bottom of the well in ImageJ using the oval tool or by freehand outlining of the gel shapes to measure the area of the entire well and that of the hydrogel. Statistical analysis for contractions was performed using one-way paired T-tests in Microsoft Excel. Expression fold differences with p-values less than 0.05 were considered significant. The following equation was used to estimate the percent contraction of the hydrogel surface:

$$Contraction \approx \left(1 - \frac{Area\ of\ gel}{Area\ of\ well}\right) x\ 100\%$$

Microarray Analysis

Gene expression of fibroblast transition through culture is a subset of data from previously published work and available through GEO accession GSE87175[17]. Protein-protein interactions were obtained using the STRING (Search Tool for Retrieval of Interacting Genes/Proteins) database. Heat map was generated using MORPHEUS from the Broad Institute. K means clustering was performed on samples via application of Euclidean distance algorithm.

RESULTS

Hydrogel Contraction is Dependent on Fibroblast Density, Fibroblast Disease Status, and ECM Protein Concentration

IPF ECM hydrogels were used for this manuscript. Hydrogels were seeded with either IPF-F or NHLF and the resulting hydrogel contraction was used as an *in vitro* proxy to evaluate fibroblast activity *in vivo*. We conducted various experiments to quantify the differential effects of fibroblast density and ECM protein concentration on hydrogel contraction. With cells seeded at concentrations of 1×10^5 (1e5), 2×10^5 (2e5), and 4×10^5 (4e5) cells per IPF derived hydrogel (ECM protein concentration 4 mg/mL) we observed an initial contraction 24 h after seeding and detected a significant difference among all three densities by 72 h (Figure 2A). For all cell densities at 4 mg/mL protein concentration, the contraction percentage plateaus at just over 80% (i.e., the hydrogels shrink to less than 20% of their original size). The 80% contraction milestone is reached just after 24 h in gels seeded with 2e5 and 4e5 fibroblasts, but with 1e5 fibroblasts the contraction exceeds 80% only after 72 h. To evaluate the impact of ECM protein concentration on contraction, we seeded 2e5 fibroblasts each in gels with ECM protein concentrations of 2, 4, and 8 mg/mL. Within 24 h, contraction is observed in 2 and 4 mg/mL gels with significant difference between 4 mg/mL and 8 mg/mL at 48 h (Figure 2B). Finally, we compared the contractile capacity of NHLF and IPF-F in 4 mg/mL hydrogels (2e5 cells per hydrogel) and observed significantly higher contraction in IPF-F-seeded hydrogels after 24 h (Figure 2C). Overall, the fibroblast cell density of 2e5 seeded in 4 mg/mL ECM protein concentration yielded the best consistency in contraction profiling. Given these results, all further experiments employed a cell density of 2e5 and ECM protein concentration of 4 mg/mL.

Fibroblasts Seeded in ECM Hydrogels Lose Activation and Proliferative Gene Expression

To evaluate the fibroblast phenotype in 3D culture, we performed qPCR using markers associated with fibroblast activation during wound healing, inflammatory signaling, and proliferation. Analysis of genes associated with fibroblast activation, including Collagen 1a1

(*COL1A1),* Smooth Muscle Actin (*ACTA2),* and Connective Tissue Growth Factor *(CTGF)*, identified a significant decrease in the activation signature of fibroblasts seeded in IPF-derived ECM gels as compared to standard 2D tissue culture plastic (Figure 3A). These observed reductions in gene expression can likely be attributed to decreased stiffness of the ECM hydrogel platform as compared to tissue culture plastic, the latter of which is a well-characterized driver of the active myofibroblast phenotype[37,38]. Further supporting this observation, we also observed a significant decrease in genes associated with proliferation in both IPF-F and NHLF (Figure 3B). We also looked at expression of the inflammation-associated genes Interleukin 6 (*IL6*), Chemokine C-C motif ligand 8 (*CCL8*), and Chemokine C-C motif ligand 7 (*CCL7*) which suggested a potential proinflammatory effect of seeding cells in the IPF hydrogels (Figure 3C). While only *CCL8* had a significant increased expression in IPF-F, this initial screening of inflammation genes presented an intriguing avenue for further characterization.

IPF Fibroblasts Seeded in Fibrotic ECM Enter a Proinflammatory State

We have previously reported that gene expression of freshly isolated lung fibroblasts is dramatically altered through extended tissue culture, and that these changes in NHLF and IPF-F result in a convergent phenotype marked by high activation as compared to the *in-vivo* state[17]. In our previous work, we specifically identified a subset of genes that were altered in both IPF-F and NHLF as the fibroblasts transitioned to tissue culture plastic. At the time we attributed those alterations to the stiff tissue culture plastic. A heat map of that data highlights two subsets of genes that are altered through tissue culture with one set increasing and one set decreasing (Figure 4A). Our focus in this manuscript is on the genes that were downregulated, or lost, upon transition to traditional 2D culture (roughly the bottom half of Figure 4A). Thus, we performed gene enrichment analysis using StringDB to identify key pathways that were not described in the previous work and identified inflammatory signaling as a major hub of genes that are

downregulated through tissue culture plastic (Figure 4B). Paired with our initial observations suggesting a potential increase of proinflammatory signaling for cells seeded in fibrotic ECM (Figure 3C), we hypothesized that the fibrotic ECM may "rescue" the inflammatory signaling that is lost upon transition to 2D tissue culture. We chose six genes from the STRING analysis: Chemokine (C-C motif) ligand 20 (*CCL20*), Chemokine (C-X-C motif) ligand 2 *(CXCL2),* Chemokine (C-X-C motif) ligand 3 (*CXCL3),* Chemokine (C-C motif) ligand 13 (*CCL13),* Chemokine (C-X-C motif) ligand 14 (*CXCL14),* and the three other inflammatory genes from above: *IL6, CCL7* and *CCL8*. Comparing NHLF and IPF-F seeded in the IPF hydrogel, we observed that IPF-F gained a significantly higher level of gene expression for many of the selected cytokines (Figure 4C). This data further supports a potential proinflammatory nature of the fibrotic ECM and suggests that IPF-F have an increased sensitivity to biochemical cues within our IPF patient-derived ECM hydrogel matrices, compared to 2D plastic.

Fibroblasts in Fibrotic ECM Activate Monocytes and Macrophages in Co-Culture

To further examine the proinflammatory state of the fibroblasts in IPF ECM, we developed a conditioned media experiment using the monocyte cell line U937 and monocyte-derived macrophages (U937s treated for 48 h with 100ng/mL PMA). We hypothesized that the increased expression of inflammatory cytokines observed in the fibrotic hydrogels would translate into the increased release of cytokines to the surrounding media of the fibroblast. Furthermore, we expected that this cytokine enriched media could elicit a potent response in either monocytes or macrophages. The assay protocol is thoroughly described in our Methods section and graphically depicted in Figure 5.

With our primary interest in fibrosis, we broadly defined cytokine panels that have previously been associated with either the inflammatory (*CD86, IL6, TNFA* and *IL1B)* or resolution (*CD163, TGFB, CCL24, and IL10)* phenotypes of macrophages in the fibrotic lung[23,25,27]. Additionally, we

also wanted to see if cytokines released from fibroblasts could promote expression of a proliferative gene set in either monocytes or macrophages. Conditioned media from fibroblasts seeded in traditional 2D tissue culture had no significant effect on monocyte gene expression across all genes tested (Figure 6A-C). However, conditioned media from NHLF and IPF-F cultured in our 3D hydrogels induced significant increases in both proinflammatory and pro-resolution gene expression in monocytes (Figure 6A-B). Expression of select genes, *CD86* and *IL10*, were significantly higher in monocytes treated with IPF-F conditioned media as compared to NHLF conditioned media, further supporting observations from above (Figure 4) suggesting that IPF-F may enter a more inflammatory state in fibrotic ECM as compared to NHLF. We also report that conditioned media from IPF-F, and not NHLF, induces expression of a proliferative gene signature in monocytes (Figure 6C).

Experiments using macrophages in co-culture once again demonstrate a differential effect when comparing conditioned media from 2D tissue culture (TC) and 3D ECM cultured fibroblasts. The proinflammatory signature was once again increased in macrophages treated with ECM conditioned media as compared to both DMEM and TC conditioned media (Figure 7A). Surprisingly, apart from *CCL24* which was significantly upregulated by ECM conditioned media, this increased expression was not observed for the profibrotic gene signature. In the case of *IL10* and *CD163*, both conditioned media permutations resulted in a decrease in the expression of these genes, with no significant difference in either *TGFB* (Figure 7B). In contrast to the effect on monocytes, the proliferative signature suggests that ECM derived conditioned media does not induce proliferation in macrophages (Figure 7C).

DISCUSSION

Since the first studies demonstrating the differential response of fibroblasts to alterations in surface stiffness[39], our growing understanding of the mechanosensing nature of the fibroblast

has been facilitated by the application of tunable matrices of varying stiffness[3,30,40–42]. The overwhelming observation, documented in numerous studies over more than 20 years, has been the induction of a smooth muscle actin expressing myofibroblast state when fibroblasts are seeded on stiff matrix and the loss of this phenotype when fibroblasts are returned to soft matrix[30,37,38,43]. However, with the incredible expansion and availability of singe cell technology, we are now acutely aware that lung mesenchyme under homeostasis and fibrotic states is comprised of variable numbers of fibroblast populations defined less by the expression of smooth muscle actin and more by the signaling cues present in their local microenvironments[44–48]. Through the application of a tunable matrix derived from fibrotic lung tissue, we contribute to the field in two important ways. First, we further confirm that lung fibroblasts are highly sensitive to their culturing environment with loss of the classical myofibroblast marker, *ACTA2*, in our 3D hydrogel (Figure 3A). Secondly, we report that the presence of ECM in the surrounding environment may be a key element to observe pathological behavior of fibroblasts *in vitro* as cells in our IPF hydrogel enter a proinflammatory state (Figure 3B and Figure 4C). Together, these two observations highlight the necessity for the development of *in vitro* models with both tunable stiffness and a biologically relevant matrix composition.

Through our initial characterization of this system, we observed that the contractile capacity of fibroblasts depends on two factors: the number of cells in the gel and the concentration of the matrix protein (Figure 2). These observations suggest that increased protein concentration in fibrotic gels increases the resistance of the gels to contractile forces exerted by seeded fibroblasts and that these contractile forces can be increased by adding more cells. We also observed that IPF-F have a greater capacity to contract the matrix as compared to NHLF seeded at the same density (Figure 2). Thus, contractility can be directly linked to the disease state, opening a new avenue for the characterization of the disease state in fibroblasts and as a potential target for evaluation of novel small molecule efficacy. Importantly, the capacity of

fibroblasts to contract was maintained despite the decreased expression of *ACTA2* and *CTGF* as compared to tissue culture plastic (Figure 3). Concurrently, these cells also lose expression of proliferation markers, strongly indicating the loss of the classical myofibroblast state.

As we characterized the altered gene expression in fibroblasts seeded in the IPF hydrogel we were struck by inflammation associated genes (Figure 3C). We have previously described altered expression of an oxidative stress induced cytokine axis when IPF fibroblasts are removed from the lung and seeded into a tissue culture dish[17]. In that work we demonstrated the sensitivity to oxidative stress and the proinflammatory state of the IPF-F under a hydrogen peroxide challenge. We went back to that same data set and interrogated a series of genes dubbed “the culture list,” these are genes that change expression in both IPF-F and NHLF when cells are isolated from the lung and seeded on tissue culture plastic (Figure 4A). In the genes that were lost during the transition to tissue culture, gene ontological enrichment analysis via StringDB identified a cytokine gene signature (Figure 4B). Interestingly, we observe that when IPF-F are seeded in the IPF hydrogels they increase gene expression of several cytokines. Together these data suggest that IPF-F in the 3D hydrogel system enter a proinflammatory phenotype and that this system potentially models an emerging role for fibroblasts as immune signaling hubs[49–53].

To better explore the potential inflammatory signaling initiated by fibroblasts in IPF ECM we developed co-culture experiments aimed to model the crosstalk between fibroblasts and immune cells. Consistent with observed increased inflammatory expression of fibroblasts cultured in IPF hydrogels (Figures 3-4), we describe differential effects when comparing monocytes and macrophages exposed to fibroblast ECM conditioned media (Figures 6-7). We broadly defined our gene signatures as either pro-inflammatory or pro-resolution. Although this classification simplifies the complex nature of monocyte and macrophage biology, it allows us to

identify intriguing differences between the monocyte and macrophage response to the conditioned media from fibroblast populations. Specifically, we clearly observed an increase of cytokine expression in monocytes treated with conditioned media from ECM fibroblasts. Independent of our pro-inflammatory or pro-resolution nomenclature, this suggests that cytokine expression within fibroblasts exposed to the fibrotic ECM is a potential signaling mechanism for activation and/or recruitment of circulating monocytes. We also observed an increase in proliferation associated gene expression, indicating that once monocytes are recruited to the site of injury, fibroblast crosstalk may also promote the expansion of the recruited monocyte population (Figure 6C). The role of monocytes recruited to the IPF lung as biomarkers and drivers of disease progression has been a topic of great interest in recent years[49,54,55] and our model suggests that the ECM itself may contribute a stimulus to initiate this crosstalk. Of particular interest, *CD86* and *IL10* expression had a significant increase in monocytes when exposed to IPF-F ECM conditioned media over the NHLF equivalent, suggesting that isolated IPF-F may retain a higher sensitivity to matrix cues (Figure 6B). IL-10, a ligand that has been implicated in monocyte-derived macrophage differentiation and IPF pathobiology [54,56–58] highlights that incoming monocytes exposed to signals from IPF-F fibroblasts may more rapidly differentiate into tissue specific macrophages. Furthermore the differential increase in CD86, a surface marker that is known to be expressed in inflammatory associated macrophages and a co-stimulatory molecule that stimulates T-cell responses [23,59], adds support to this accelerated crosstalk. As a future scope of this work, additional studies applying omics technology are required to thoroughly investigate the biological implications of these observations.

The conditioned media challenge in macrophages had a similar effect though there were some important differences. As before the conditioned media derived from both ECM seeded fibroblasts continued to increase the pro-inflammatory signature in macrophages. However, the genes listed as pro-resolution were either decreased or unaffected, save for CCL24 (Figure 7A-

B). Overall, this challenge supports the hypothesis that fibroblasts seeded in IPF ECM are primed to secrete cytokines that drive an inflammatory monocyte and/or macrophage phenotype. Speaking directly to CCL24, an eotaxin that has recently been implicated in IPF biology and a novel therapeutic target[56,60,61], this increased expression highlights the shortcomings of broadly classifying cytokines into pro-inflammatory or pro-resolution. As an eotaxin, CCL24 is primarily implicated in the recruitment to and activation of eosinophils at sites of inflammation. While debate on the role of eosinophils as pro-inflammatory or pro-resolution remains outside the scope of this work, we suggest that this observation further supports our argument of the fibrotic ECM promoting a signaling pathway in fibroblasts that serves to recruit and activate the lung monocyte and macrophage populations.

Taken together, our findings suggest that there are properties inherent to the hydrogel system that induce a less classically active, but more inflammatory fibroblast than those grown on tissue culture plastic. We see this inflammatory signature in the fibroblast and its crosstalk with immune cells which imply that fibrotic ECM, by its nature, induces inflammatory cues that further exacerbate this disease. This inflammatory property is likely attributed to the protein composition of the matrix and the mechanical properties of the gel, a promising sign that fibrotic hydrogels recapitulate aspects of the *in vivo* lung environment that are not captured by tissue culture plastic. Given that the matrix conditions were the same for both cell types, these data support previous findings from our group, and others, describing disease associated fibroblast alterations to their functional biology[16,17]. Fibrotic ECM hydrogels provide a new way of assessing fibroblasts and diseases associated with matrix remodeling. By developing materials for fibroblast culture that mimic physiological conditions, we hope to expand knowledge on novel pathways toward screening, discovery, and approval of more efficacious antifibrotic therapeutics.

AUTHOR CONTRIBUTIONS

LR, GG, JLM conceived and designed research; JFD, DM, JK, JAK, AKS, ML performed experiments and collected samples; JFD, DM, AKS, SD, LR, GG, JLM analyzed data and interpreted results; JFD generated figures and drafted the manuscript; JFD, AKS, CSK, SD, LR, GG, JLM revised the manuscript; all authors reviewed and approved the final version.

ACKNOWLEDGMENTS

The authors would like to thank all the patients that donated their tissue and allowed this work to be done. We also extend our gratitude to the clinical coordinators at Inova who reached out and obtained approval from all the patients. Finally, we to thank Amy Carfagno, Ammal H Altalhi, Dr. Tom Huff and Tabitha King for their technical guidance.

FUNDING

This research was supported by grant funding from Virginia's Commonwealth Health Research Board.

DISCLOSURES

No conflicts of interest, financial or otherwise, are declared by the authors.

FIGURE LEGENDS

Figure 1 Schematics of IPF hydrogel synthesis protocol: Procured human lung tissue is minced (1) and decellularized with ionic detergent washes and DNase to remove extracellular DNA (2). Scaffold is sterilized with ethanol followed by a lyophilization (3). The scaffold is pulverized (4) and then digested with pepsin (5), followed by a dialysis (6), and finalized by a secondary lyophilization (7). Powder is resuspended with culture media and seeded with cells. Gelation of sample occurs at 37°C (8,9).

Figure 2 Contraction Rate of IPF Derived Hydrogels (A1) IPF hydrogel (4 mg/mL ECM protein concentration) seeded with varying fibroblast densities: 1e5, 2e5, and 4e5 cells/well. (A2) Bar graph demonstrating a significant increase at all time points in hydrogel contraction as cell density increases. (B1) IPF hydrogel at varying ECM protein concentrations: 2 mg/mL, 4 mg/mL, and 8 mg/mL with a fibroblast density of 2e5 cells/well. (B2) Bar graph demonstrating a significant decrease of hydrogel contractions at all time points as concentration of IPF ECM in the hydrogel increases. (C1) IPF hydrogel seeded with IPF fibroblasts (IPF-F) and normal human lung fibroblasts (NHLF), imaged after 24 h. (C2) Significantly increased contraction of IPF-F in comparison to NHLF in IPF hydrogels after 24 h. *: $p<0.05$, **: $p<0.005$, ***: $p<0.0005$, ****: $p<0.00005$, *****: $p<0.000005$.

Figure 3 Gene Expression of IPF-F and NHLF Fibroblasts Seeded in IPF Hydrogel and Tissue Culture Plastic. (A) Gene expression of fibroblast activation markers: *Col1a1, ACTA2,* and *CTGF*. (B) Gene expression of ligands associated with inflammation: *IL6, CCL8, and CCL7 (*C) Gene expression of markers associated with cell proliferation: *TOP2A* and *MKI67*. *: $p<0.05$.

*Figure 4 Proinflammatory Gene Expression of Fibroblast in Fibrotic ECM Hydrogel (*A) Microarray data highlighting gene expression changes of fibroblasts immediately prior to culture and after 3 weeks. (B) STRING analysis of protein interactions compiled from genes in the bottom block of the heat map in Figure 4A. (C) Bar graphs demonstrating fold change of gene expression *(CCL20, CXCL2, CXCL3, CXCL13, CXCL14, CXCR4)* from STRING diagram in Figure 4B comparing NHLF and IPF-F seeded in IPF hydrogels against the average of NHLF expression*. IL6, CCL7* and *CCL8* are not part of the genes in STRING diagram but were identified as inflammatory genes in Figure 3B. *: $p<0.05$.

Figure 5 Schematic Depiction of Conditioned Media Experiments. Fibroblasts are seeded in IPF hydrogels for 48 h (1) and culture conditioned media is collected and used to culture U937s, and PMA treated U937s (2). U937 cultures are taken down after 48 h for RNA isolation and qPCR (3).

Figure 6 Gene Expression of Monocytes After Fibroblast Conditioned Media Challenge. (A) Gene expression fold change of pro-inflammatory genes: *CD86*, *IL6*, *TNFA*, and *IL1B* (B) Gene expression fold change of pro-resolution genes: *CD163*, *TGF-B*, *CCL24*, *IL10*. (C) Gene expression fold change of markers cell cycle and proliferation: *TOP2A*, *PCNA*, and *P16.* *: $p<0.05$, **: $p<0.005$, ***: $p<0.0005$, ****: $p<0.00005$.

Figure 7: Gene Expression of Monocyte-Derived Macrophages After Fibroblast Conditioned Media Challenge. (A) Gene expression fold change of pro-inflammatory genes: *CD86*, *IL6*, *TNF-a*, and *IL1B* (B) Gene expression fold change of pro-resolution genes: *CD163*, *TGF-B*, *CCL24*, *IL10*. (C) Gene expression fold change of markers cell cycle and proliferation: *TOP2A*, *PCNA*, and *P16.* *: $p<0.05$, **: $p<0.005$, ***: $p<0.0005$, ****: $p<0.00005$.

REFERENCES

1. Betensley, A., Sharif, R. & Karamichos, D. A Systematic Review of the Role of Dysfunctional Wound Healing in the Pathogenesis and Treatment of Idiopathic Pulmonary Fibrosis. *J. Clin. Med.* **6**, 2 (2016).
2. Sgalla, G. *et al.* Idiopathic pulmonary fibrosis: pathogenesis and management. *Respir. Res.* **19**, (2018).
3. Smithmyer, M. E., Sawicki, L. A. & Kloxin, A. M. Hydrogel scaffolds as in vitro models to study fibroblast activation in wound healing and disease. *Biomater. Sci.* **2**, 634–650 (2014).

4. Moretti, L., Stalfort, J., Barker, T. H. & Abebayehu, D. The interplay of fibroblasts, the extracellular matrix, and inflammation in scar formation. *J. Biol. Chem.* **298**, 101530 (2022).
5. Margaritopoulos, G. A., Vasarmidi, E. & Antoniou, K. M. Pirfenidone in the treatment of idiopathic pulmonary fibrosis: an evidence-based review of its place in therapy. *Core Evid.* **11**, 11–22 (2016).
6. Vancheri, C. *et al.* Nintedanib with Add-on Pirfenidone in Idiopathic Pulmonary Fibrosis. Results of the INJOURNEY Trial. *Am. J. Respir. Crit. Care Med.* **197**, 356–363 (2018).
7. Wollin, L. *et al.* Mode of action of nintedanib in the treatment of idiopathic pulmonary fibrosis. *Eur. Respir. J.* **45**, 1434–1445 (2015).
8. Sgalla, G., Lerede, M. & Richeldi, L. Phase three clinical trials in idiopathic pulmonary fibrosis. *Expert Opin. Orphan Drugs* **9**, 1–11 (2021).
9. Flaherty, K. R. *et al.* Nintedanib in Progressive Fibrosing Interstitial Lung Diseases. *N. Engl. J. Med.* **381**, 1718–1727 (2019).
10. Noble, P. W. *et al.* Pirfenidone in patients with idiopathic pulmonary fibrosis (CAPACITY): two randomised trials. *The Lancet* **377**, 1760–1769 (2011).
11. Aimo, A. *et al.* Pirfenidone is a cardioprotective drug: Mechanisms of action and preclinical evidence. *Pharmacol. Res.* **155**, 104694 (2020).
12. Ahluwalia, N., Shea, B. S. & Tager, A. M. New Therapeutic Targets in Idiopathic Pulmonary Fibrosis. Aiming to Rein in Runaway Wound-Healing Responses. *Am. J. Respir. Crit. Care Med.* **190**, 867–878 (2014).
13. Woodley, J. P., Lambert, D. W. & Asencio, I. O. Understanding Fibroblast Behavior in 3D Biomaterials. *Tissue Eng. Part B Rev.* (2021) doi:10.1089/ten.teb.2021.0010.
14. Evangelista-Leite, D., Carreira, A. C. O., Gilpin, S. E. & Miglino, M. A. Protective Effects of Extracellular Matrix-Derived Hydrogels in Idiopathic Pulmonary Fibrosis. *Tissue Eng. Part B Rev.* (2021) doi:10.1089/ten.teb.2020.0357.

15. Kapałczyńska, M. *et al.* 2D and 3D cell cultures – a comparison of different types of cancer cell cultures. *Arch. Med. Sci. AMS* **14**, 910–919 (2018).
16. Emblom-Callahan, M. C. *et al.* Genomic phenotype of non-cultured pulmonary fibroblasts in idiopathic pulmonary fibrosis. *Genomics* **96**, 134–145 (2010).
17. Rodriguez, L. R. *et al.* Global Gene Expression Analysis in an in vitro Fibroblast Model of Idiopathic Pulmonary Fibrosis Reveals Potential Role for CXCL14/CXCR4. *Sci. Rep.* **8**, 3983 (2018).
18. Nemeth, J., Schundner, A., Quast, K., Winkelmann, V. E. & Frick, M. A Novel Fibroblast Reporter Cell Line for in vitro Studies of Pulmonary Fibrosis. *Front. Physiol.* **11**, (2020).
19. Vazquez-Armendariz, A. I., Barroso, M. M., El Agha, E. & Herold, S. 3D In Vitro Models: Novel Insights into Idiopathic Pulmonary Fibrosis Pathophysiology and Drug Screening. *Cells* **11**, 1526 (2022).
20. Huang, R. Y.-J., Guilford, P. & Thiery, J. P. Early events in cell adhesion and polarity during epithelial-mesenchymal transition. *J. Cell Sci.* **125**, 4417–4422 (2012).
21. Herrera, J., Henke, C. A. & Bitterman, P. B. Extracellular matrix as a driver of progressive fibrosis. *J. Clin. Invest.* **128**, 45–53.
22. de Hilster, R. H. J. *et al.* Human lung extracellular matrix hydrogels resemble the stiffness and viscoelasticity of native lung tissue. *Am. J. Physiol. - Lung Cell. Mol. Physiol.* **318**, L698–L704 (2020).
23. Zhang, L. *et al.* Macrophages: friend or foe in idiopathic pulmonary fibrosis? *Respir. Res.* **19**, 170 (2018).
24. Ogawa, T., Shichino, S., Ueha, S. & Matsushima, K. Macrophages in lung fibrosis. *Int. Immunol.* **33**, 665–671 (2021).
25. Cheng, P., Li, S. & Chen, H. Macrophages in Lung Injury, Repair, and Fibrosis. *Cells* **10**, 436 (2021).

26. Sica, A. & Mantovani, A. Macrophage plasticity and polarization: in vivo veritas. *J. Clin. Invest.* **122**, 787–795 (2012).
27. Arora, S., Dev, K., Agarwal, B., Das, P. & Syed, M. A. Macrophages: Their role, activation and polarization in pulmonary diseases. *Immunobiology* **223**, 383–396 (2018).
28. Kishore, A. & Petrek, M. Roles of Macrophage Polarization and Macrophage-Derived miRNAs in Pulmonary Fibrosis. *Front. Immunol.* **12**, (2021).
29. Ullm, F. *et al.* 3D Scaffold-Based Macrophage Fibroblast Coculture Model Reveals IL-10 Dependence of Wound Resolution Phase. *Adv. Biosyst.* **4**, 1900220 (2020).
30. Matera, D. L. *et al.* Microengineered 3D pulmonary interstitial mimetics highlight a critical role for matrix degradation in myofibroblast differentiation. *Sci. Adv.* **6**, eabb5069 (2020).
31. Kono, T. *et al.* Cell cycle analysis of human dermal fibroblasts cultured on or in hydrated type I collagen lattices. *Arch. Dermatol. Res.* **282**, 258–262 (1990).
32. Denton, C. P. *et al.* Therapeutic interleukin-6 blockade reverses transforming growth factor-beta pathway activation in dermal fibroblasts: insights from the faSScinate clinical trial in systemic sclerosis. *Ann. Rheum. Dis.* **77**, 1362–1371 (2018).
33. Kumari, J., Wagener, F. A. D. T. G. & Kouwer, P. H. J. Novel Synthetic Polymer-Based 3D Contraction Assay: A Versatile Preclinical Research Platform for Fibrosis. *ACS Appl. Mater. Interfaces* **14**, 19212–19225 (2022).
34. Mattyasovszky, S. G. *et al.* Influence of the anti-inflammatory cytokine interleukin-4 on human joint capsule myofibroblasts. *J. Orthop. Res.* **35**, 1290–1298 (2017).
35. Freytes, D. O., Martin, J., Velankar, S. S., Lee, A. S. & Badylak, S. F. Preparation and rheological characterization of a gel form of the porcine urinary bladder matrix. *Biomaterials* **29**, 1630–1637 (2008).
36. Pfaffl, M. W. A new mathematical model for relative quantification in real-time RT–PCR. *Nucleic Acids Res.* **29**, e45 (2001).

37. Dasgupta, I. & McCollum, D. Control of cellular responses to mechanical cues through YAP/TAZ regulation. *J. Biol. Chem.* **294**, 17693–17706 (2019).

38. Scott, K. E., Fraley, S. I. & Rangamani, P. A spatial model of YAP/TAZ signaling reveals how stiffness, dimensionality, and shape contribute to emergent outcomes. *Proc. Natl. Acad. Sci.* **118**, e2021571118 (2021).

39. Arora, P. D., Narani, N. & McCulloch, C. A. G. The Compliance of Collagen Gels Regulates Transforming Growth Factor-β Induction of α-Smooth Muscle Actin in Fibroblasts. *Am. J. Pathol.* **154**, 871–882 (1999).

40. Liu, F. *et al.* Mechanosignaling through YAP and TAZ drives fibroblast activation and fibrosis. *Am. J. Physiol.-Lung Cell. Mol. Physiol.* **308**, L344–L357 (2014).

41. Huang, X. *et al.* Matrix Stiffness–Induced Myofibroblast Differentiation Is Mediated by Intrinsic Mechanotransduction. *Am. J. Respir. Cell Mol. Biol.* **47**, 340–348 (2012).

42. Wipff, P.-J. & Hinz, B. Myofibroblasts work best under stress. *J. Bodyw. Mov. Ther.* **13**, 121–127 (2009).

43. D'Urso, M. & Kurniawan, N. A. Mechanical and Physical Regulation of Fibroblast–Myofibroblast Transition: From Cellular Mechanoresponse to Tissue Pathology. *Front. Bioeng. Biotechnol.* **8**, 609653 (2020).

44. Zepp, J. A. *et al.* Distinct mesenchymal lineages and niches promote epithelial self-renewal and myofibrogenesis in the lung. *Cell* **170**, 1134-1148.e10 (2017).

45. Adams, T. S. *et al.* Single Cell RNA-seq reveals ectopic and aberrant lung resident cell populations in Idiopathic Pulmonary Fibrosis. *bioRxiv* 759902 (2019) doi:10.1101/759902.

46. Reyfman, P. A. *et al.* Single-Cell Transcriptomic Analysis of Human Lung Provides Insights into the Pathobiology of Pulmonary Fibrosis. *Am. J. Respir. Crit. Care Med.* **199**, 1517–1536 (2019).

47. Tsukui, T. *et al.* Collagen-producing lung cell atlas identifies multiple subsets with distinct localization and relevance to fibrosis. *Nat. Commun.* **11**, 1920 (2020).

48. Buechler, M. B. *et al.* Cross-tissue organization of the fibroblast lineage. *Nature* **593**, 575–579 (2021).

49. Kolahian, S., Fernandez, I. E., Eickelberg, O. & Hartl, D. Immune Mechanisms in Pulmonary Fibrosis. *Am. J. Respir. Cell Mol. Biol.* **55**, 309–322 (2016).

50. Moss, B. J., Ryter, S. W. & Rosas, I. O. Pathogenic Mechanisms Underlying Idiopathic Pulmonary Fibrosis. *Annu. Rev. Pathol. Mech. Dis.* **17**, 515–546 (2022).

51. Österreicher, C. H. *et al.* Fibroblast-specific protein 1 identifies an inflammatory subpopulation of macrophages in the liver. *Proc. Natl. Acad. Sci.* **108**, 308–313 (2011).

52. Sundararaj, K. P. *et al.* Interleukin-6 Released from Fibroblasts Is Essential for Up-regulation of Matrix Metalloproteinase-1 Expression by U937 Macrophages in Coculture. *J. Biol. Chem.* **284**, 13714–13724 (2009).

53. Xu, Q. *et al.* The role of macrophage–fibroblast interaction in lipopolysaccharide-induced pulmonary fibrosis: an acceleration in lung fibroblast aerobic glycolysis. *Lab. Invest.* **102**, 432–439 (2022).

54. Greiffo, F., Fernandez, I., Frankenberger, M., Behr, J. & Eickelberg, O. Circulating monocytes from interstitial lung disease patients show an activated phenotype. *Eur. Respir. J.* **48**, (2016).

55. Kreuter, M. *et al.* Monocyte Count as a Prognostic Biomarker in Patients with Idiopathic Pulmonary Fibrosis. *Am. J. Respir. Crit. Care Med.* **204**, 74–81 (2021).

56. Foster, M. W. *et al.* Quantitative Proteomics of Bronchoalveolar Lavage Fluid in Idiopathic Pulmonary Fibrosis. *J. Proteome Res.* **14**, 1238–1249 (2015).

57. Millar, A. B. IL-10: another therapeutic target in idiopathic pulmonary fibrosis? *Thorax* **61**, 835–836 (2006).

58. She, Y. X., Yu, Q. Y. & Tang, X. X. Role of interleukins in the pathogenesis of pulmonary fibrosis. *Cell Death Discov.* **7**, 1–10 (2021).

59. Lis-López, L., Bauset, C., Seco-Cervera, M. & Cosín-Roger, J. Is the Macrophage Phenotype Determinant for Fibrosis Development? *Biomedicines* **9**, 1747 (2021).

60. Mor, A. *et al.* Blockade of CCL24 with a monoclonal antibody ameliorates experimental dermal and pulmonary fibrosis. *Ann. Rheum. Dis.* **78**, 1260–1268 (2019).

61. Kohan, M., Puxeddu, I., Reich, R., Levi-Schaffer, F. & Berkman, N. Eotaxin-2/CCL24 and eotaxin-3/CCL26 exert differential profibrogenic effects on human lung fibroblasts. *Ann. Allergy. Asthma. Immunol.* **104**, 66–72 (2010).

Figure 1

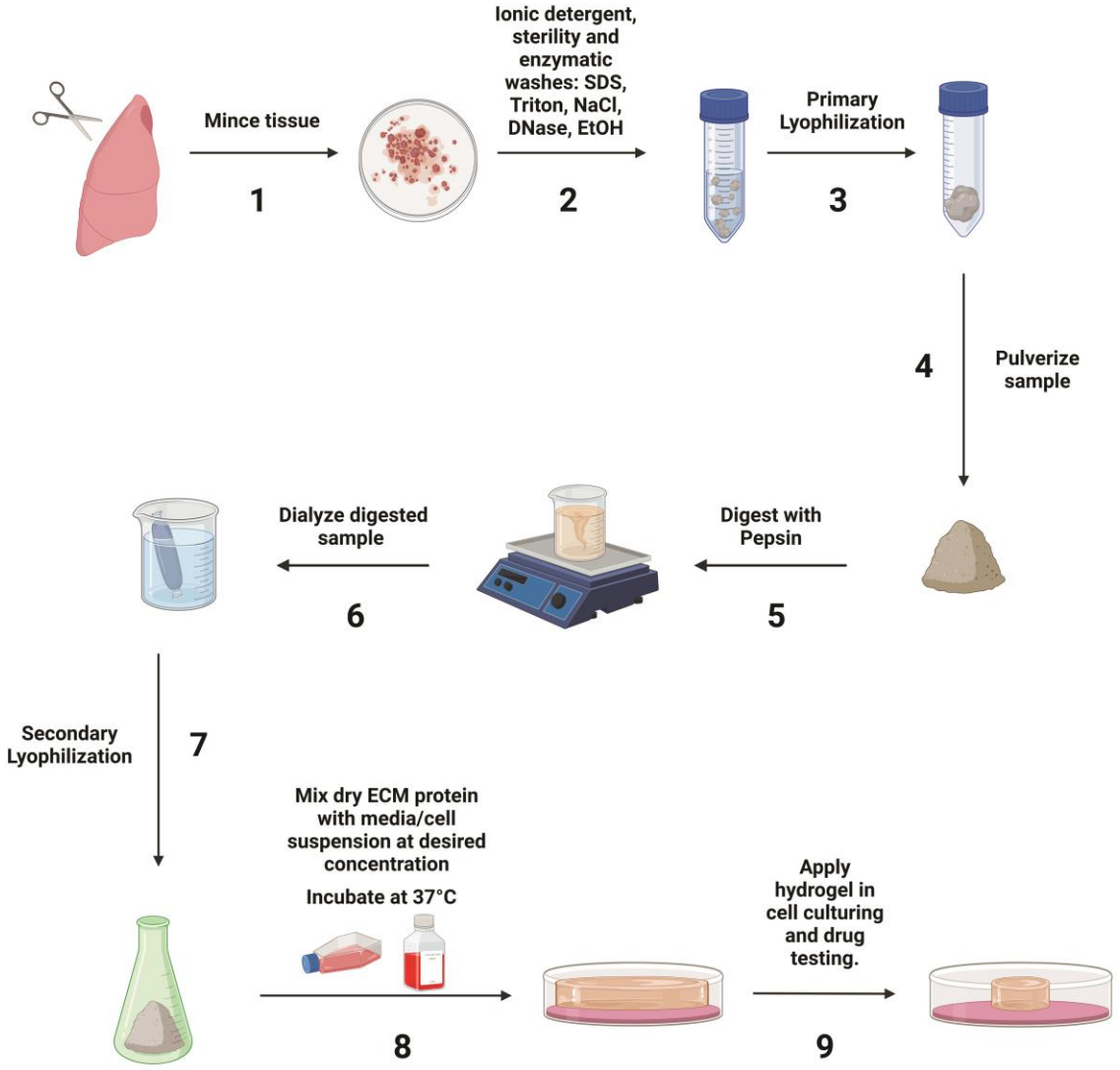
Mince tissue
1
Ionic detergent, sterility and enzymatic washes: SDS, Triton, NaCl, DNase, EtOH
2
Primary Lyophilization
3
4
Pulverize sample
Digest with Pepsin
5
Dialyze digested sample
6
Secondary Lyophilization
7
Mix dry ECM protein with media/cell suspension at desired concentration
Incubate at 37°C
8
Apply hydrogel in cell culturing and drug testing.
9

Figure 2

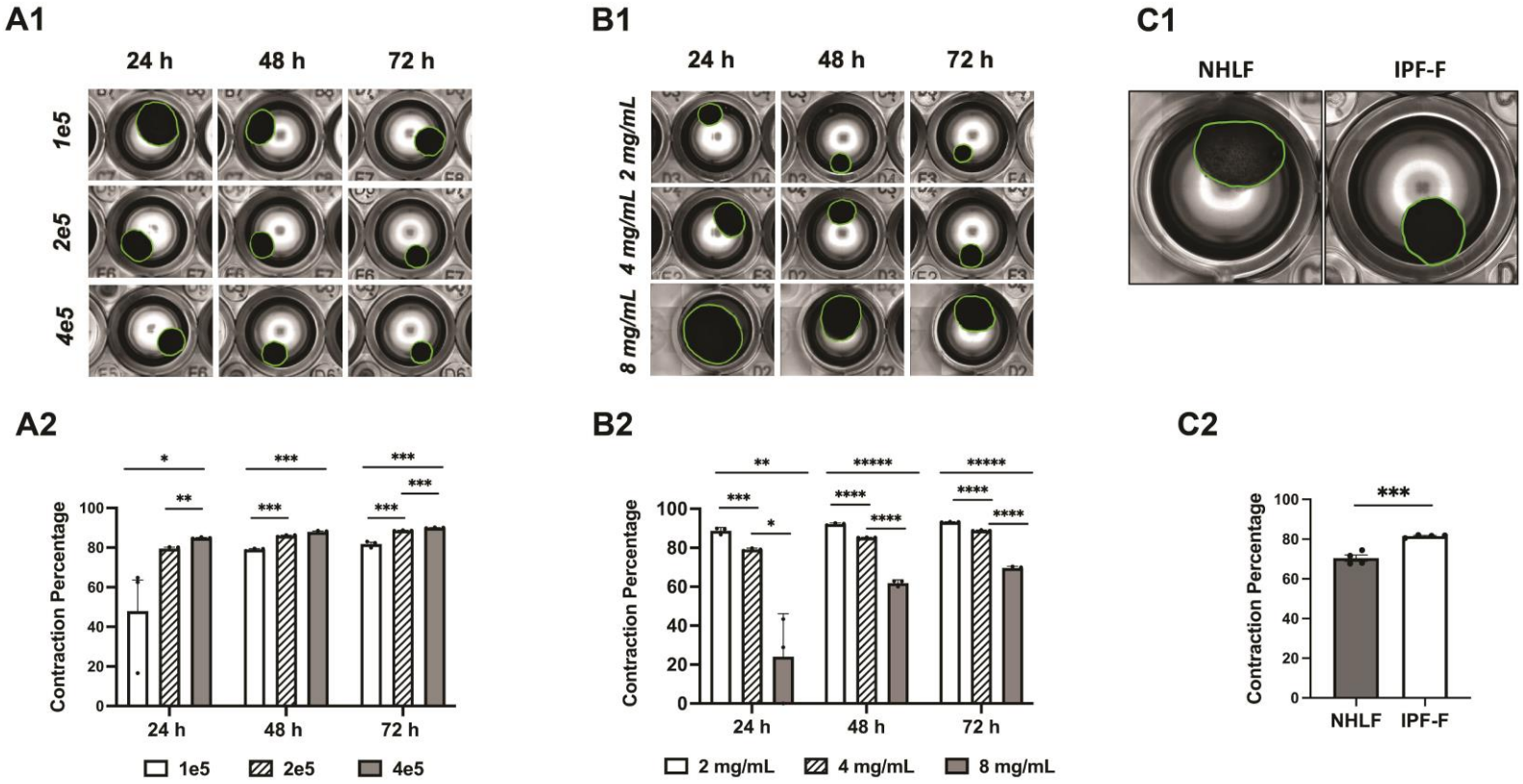
A1
24 h
48 h
72 h
1e5
2e5
4e5
B1
24 h
48 h
72 h
2 mg/mL
4 mg/mL
8 mg/mL
C1
NHLF
IPF-F
A2
Contraction Percentage
24 h
48 h
72 h
1e5
2e5
4e5
B2
Contraction Percentage
24 h
48 h
72 h
2 mg/mL
4 mg/mL
8 mg/mL
C2
Contraction Percentage
NHLF
IPF-F

Figure 3

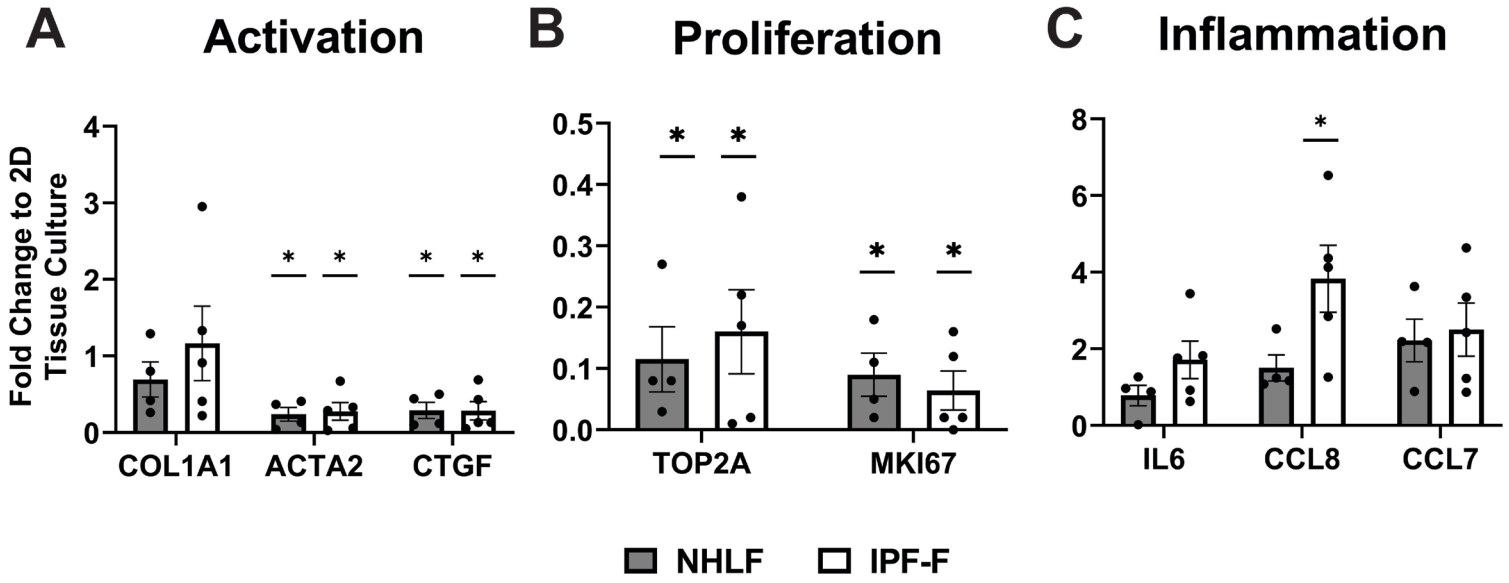
A
Activation
B
Proliferation
C
Inflammation
Fold Change to 2D Tissue Culture
COL1A1
ACTA2
CTGF
TOP2A
MKI67
IL6
CCL8
CCL7
NHLF
IPF-F

Figure 4

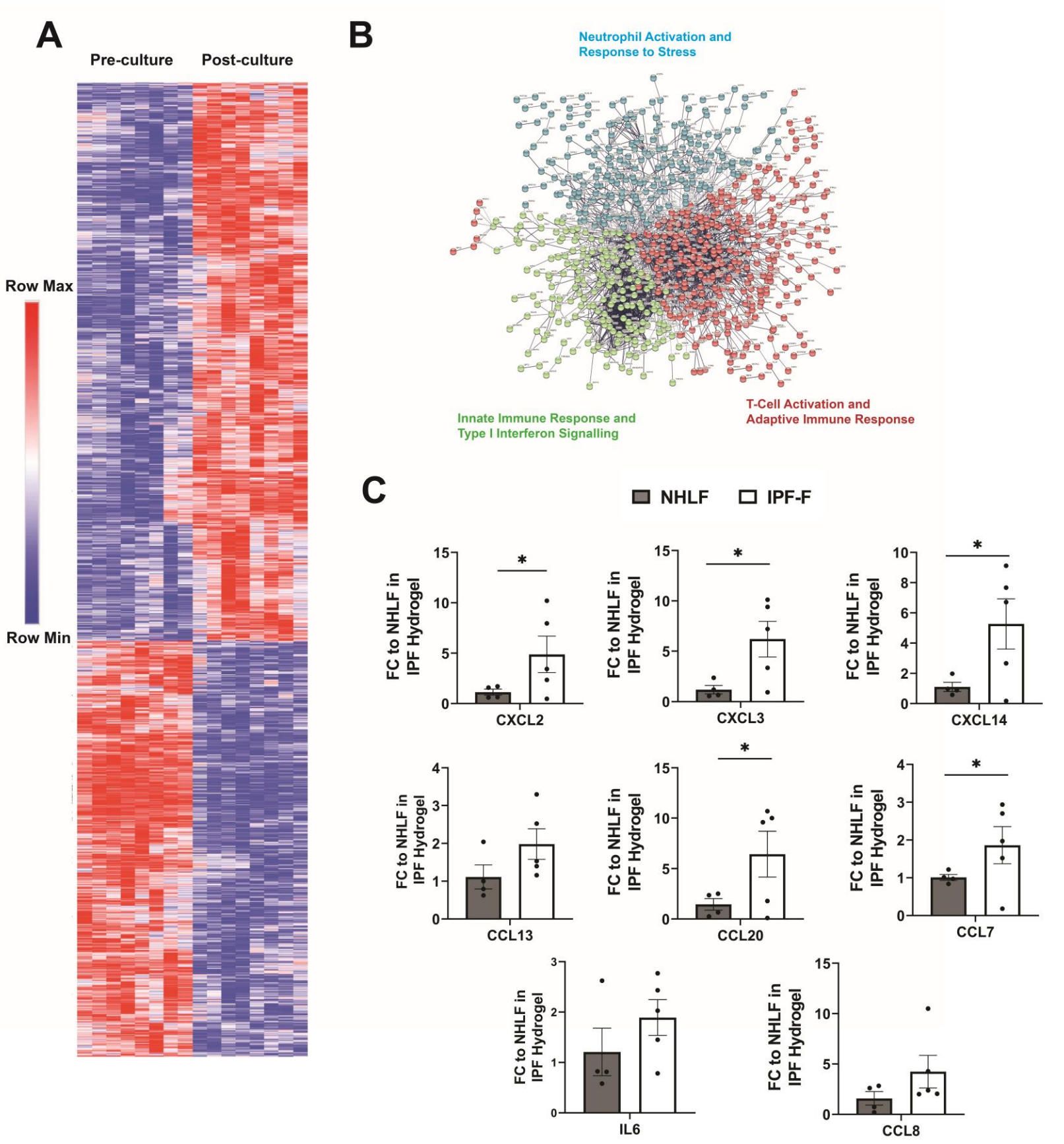
A
Pre-culture
Post-culture
Row Max
Row Min
B
Neutrophil Activation and Response to Stress
Innate Immune Response and Type I Interferon Signalling
T-Cell Activation and Adaptive Immune Response
C
NHLF
IPF-F
FC to NHLF in IPF Hydrogel
CXCL2
CXCL3
CXCL14
CCL13
CCL20
CCL7
IL6
CCL8
*

Figure 5

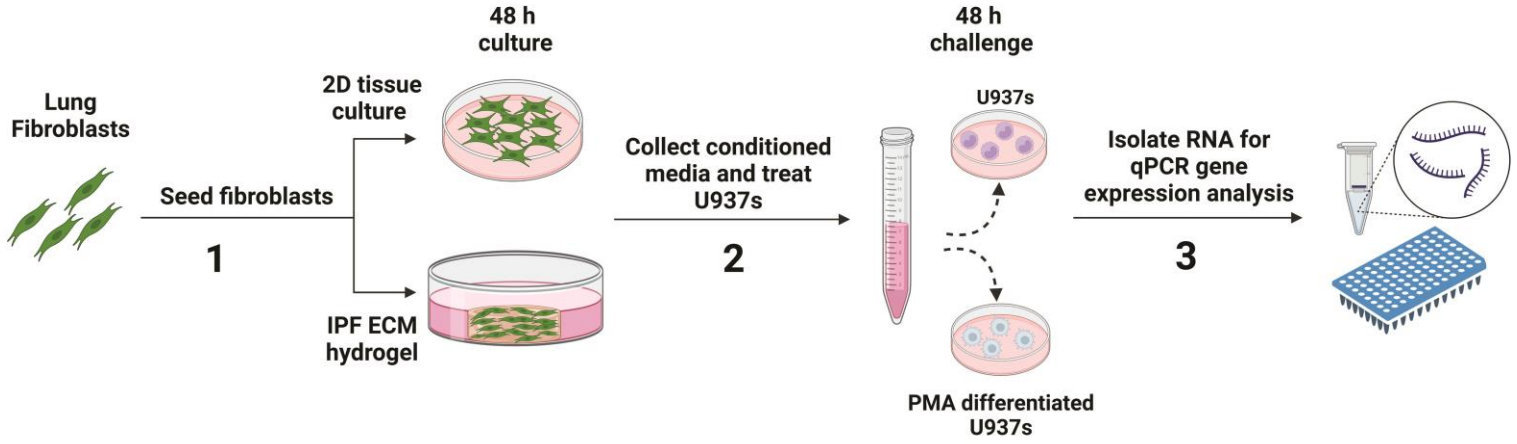
Lung Fibroblasts
Seed fibroblasts
1
2D tissue culture
48 h culture
IPF ECM hydrogel
Collect conditioned media and treat U937s
2
48 h challenge
U937s
PMA differentiated U937s
Isolate RNA for qPCR gene expression analysis
3

Figure 6

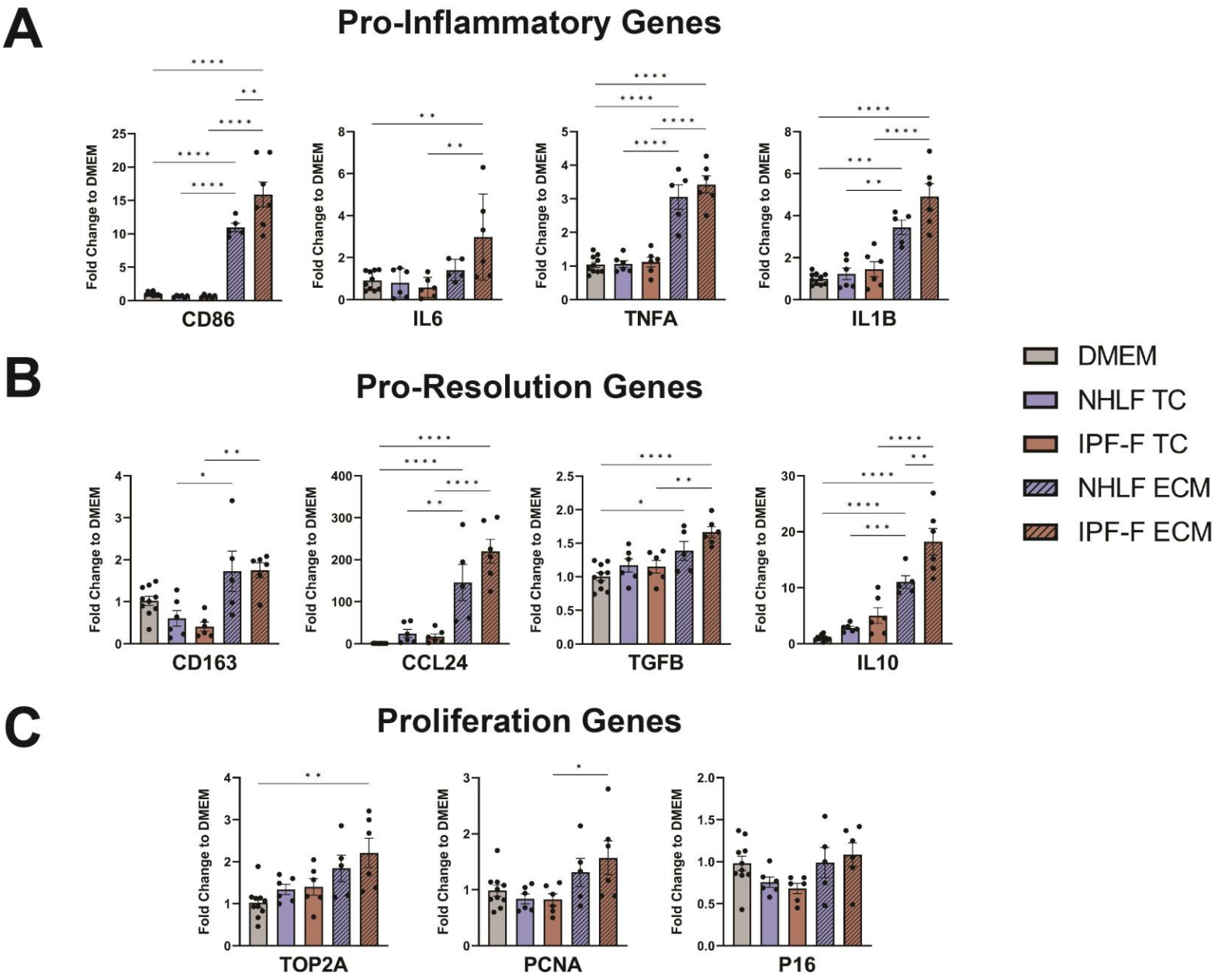
A
Pro-Inflammatory Genes
Fold Change to DMEM
CD86
IL6
TNFA
IL1B
B
Pro-Resolution Genes
CD163
CCL24
TGFB
IL10
C
Proliferation Genes
TOP2A
PCNA
P16
DMEM
NHLF TC
IPF-F TC
NHLF ECM
IPF-F ECM

Figure 7

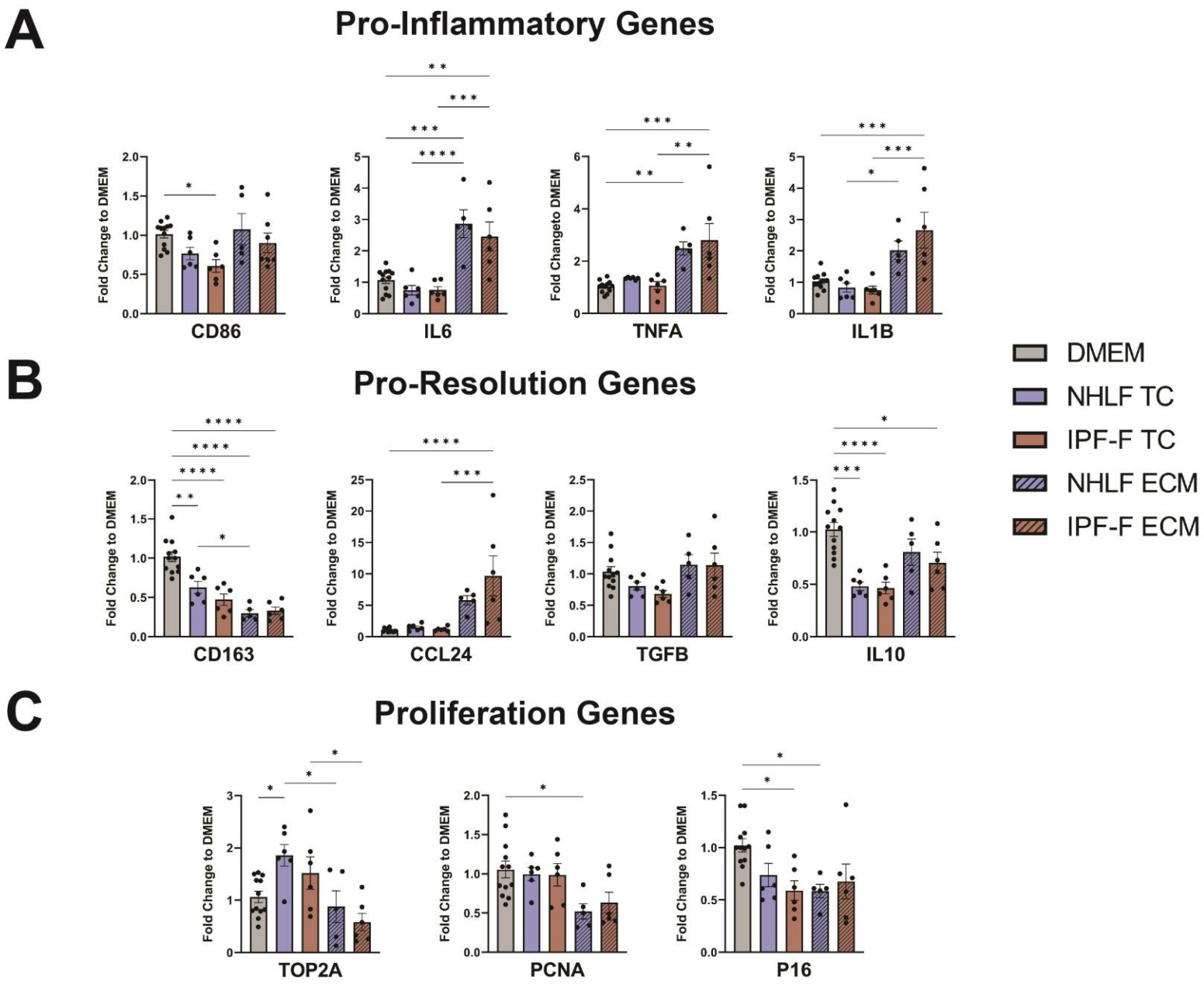
A
Pro-Inflammatory Genes
Fold Change to DMEM
CD86
IL6
TNFA
IL1B
B
Pro-Resolution Genes
CD163
CCL24
TGFB
IL10
C
Proliferation Genes
TOP2A
PCNA
P16
DMEM
NHLF TC
IPF-F TC
NHLF ECM
IPF-F ECM